

Dielectric Behavior of Epoxy/BaTiO₃ Composites Using Nanostructured Ceramic Fibers Obtained by Electrospinning

H. A. Ávila,^{*†} L. A. Ramajo,[†] M. S. Góes,[‡] M. M. Reboredo,[†] M. S. Castro,[†] and R. Parra[†]

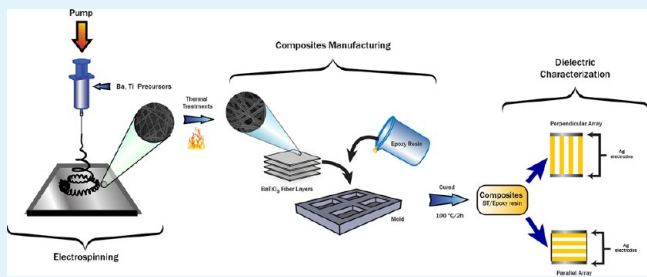
[†]Instituto de Investigaciones en Ciencia y Tecnología de Materiales (INTEMA), CONICET – UNMdP, J. B. Justo 4302, B7608FDQ – Mar del Plata, Argentina

[‡]Instituto de Química, UNESP, Rua F. Degni s/n, 14800 – Araraquara, Brasil

ABSTRACT: Composite materials made of epoxy resin and barium titanate (BT) electrospun nanostructured fibers were prepared. BT fibers were synthesized from a sol based on barium acetate, titanium isopropoxide, and poly(vinyl pyrrolidone). The fibers were heat-treated at different temperatures and characterized by X-ray diffraction, scanning electron microscopy (SEM), and Raman spectroscopy. Mats of BT fibers heat-treated at 800 °C were embedded in epoxy resin into suitable molds. The composites were characterized by SEM, and dielectric measurements were performed by means of dielectric spectroscopy.

The dielectric permittivity and dielectric modulus of epoxy resin/BT-fiber composites were measured for two types of samples: with the electrodes parallel and perpendicular to the BT fiber layers. Interestingly, composite samples with electrodes perpendicular to the fiber layers and a BT content as low as 2 vol % led to dielectric permittivities three times higher than that of pure epoxy resin.

KEYWORDS: BaTiO₃, composites, epoxy resin, dielectric permittivity, electrospinning



INTRODUCTION

With the ongoing drive towards device miniaturization, it is crucial to gain control of the synthesis and processability of materials in the nanoscale. In the past few years, one-dimensional (1D) materials such as nanofibers, nanowires, and nanorods have attracted attention because they can be used as building blocks for devices with a wide range of applications. In particular, nanofibers can be produced by simple methods like electrospinning.^{1–5} For instance, some polymer nanofibers have been synthesized by this technique, from cellulose and its derivatives,^{6–8} poly(vinyl alcohol) (PVA), poly(vinyl pyrrolidone) (PVP), poly(ethyleneoxide) (PEO), polyamides, and many other polymers.⁴ Recently, research has focused on the production of metal oxide/polymer and metal oxide fibers for diverse applications. In the case of metal oxide nanofibers, attention should be given to the necessary calcination steps to achieve burning of the polymer and of the organic additives as well as to the crystallization of the desired ceramic phase.⁹ Among ceramic materials, photoluminescent CdTe/PVP fibers,¹⁰ TiO₂,¹¹ porous TiO₂ and BaMnO₃ fibers,^{12,13} SnO₂ and TiO₂ fiber gas sensors,^{14–16} bicomponent SnO₂–TiO₂ photo-catalytic fibers,¹⁷ and Ce–Y₂O₃¹⁸ and BaTiO₃ hollow fibers¹⁹ have been all synthesized by electrospinning techniques.

Specifically, barium titanate fibers have been synthesized by electrospinning with promising results by many research groups.^{19–28} However, the application of these fibers to electronic devices and assessment of the resulting properties beyond microstructural characterization have been rarely reported. To date, BaTiO₃ fibers have been used in humidity sensors²⁵ and ferroelectric measurements have been carried out on BaTiO₃/PVDF composite fibers.²⁹

Composite materials consist of two or more phases mixed in determined proportions in order to obtain enhanced performances with respect to the isolated components. The increasing demand for low-cost and small size electronic devices has promoted the development of new ceramic–polymer composites.^{30,31} Polymers filled with certain ceramic powders are promising materials for embedded capacitors, which combine the high dielectric constant of the ceramic with the easy processability of polymers.^{32–34} Thus, BaTiO₃/epoxy composites used for embedded capacitor films (ECFs) have been extensively studied because of the simple and convenient fabrication process, low cost, and excellent properties such as low dielectric loss, low conductivity and leakage current, and compatibility with printed wiring boards (PWBs).^{32,35–38}

In this work, barium titanate nanofibers were synthesized via sol–gel and electrospinning. Composite materials for electronic applications, with low ceramic content, were prepared by alternating layers of fibers in an epoxy resin matrix. So far, the dielectric properties of BT electrospun fibers or composites consisting of epoxy resin/BT-fibers have not been reported in the literature. The influence of the electrode configuration with respect to the barium titanate fiber layers on the dielectric response of the composites is discussed in this work.

EXPERIMENTAL PROCEDURE

BaTiO₃ (BT) nanofibers were prepared as follows: barium acetate (Mallinckrodt) was dissolved in glacial acetic acid (Merk) and mixed

Received: March 27, 2012

Accepted: January 2, 2013

Published: January 2, 2013

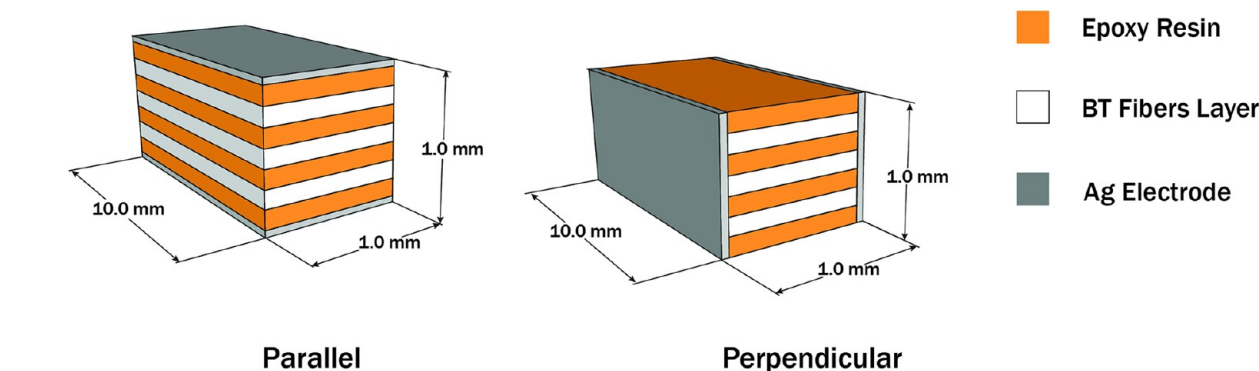


Figure 1. Schematic drawings of epoxy/BaTiO₃-fiber composites showing different electrode configurations.

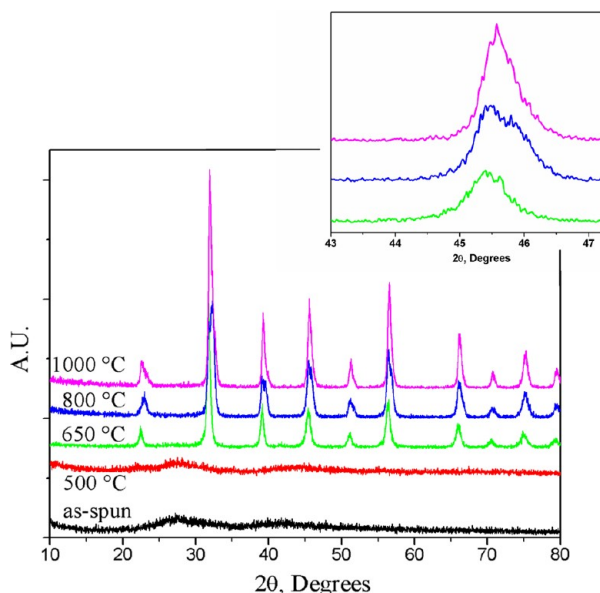


Figure 2. XRD patterns of PVP/BT fibers heat-treated at different temperatures. Inset shows a magnification of the 43.0–47.5° 2θ region for crystalline samples.

under vigorous stirring inside a glovebox with titanium isopropoxide (Aldrich, 97%) stabilized by a solution of acetylacetone (Aldrich, 99.9%) in absolute ethanol (Cicarelli). The obtained sol was mixed with a solution of 0.16 g of poly(vinyl pyrrolidone) (PVP, 1.3 MDa, Aldrich) in 3 mL of absolute ethanol. For electrospinning, the sol was loaded into a plastic syringe. A DC voltage of 13 kV was applied to the needle by a power supply unit (Gamma High Voltage Research, 0–30 kV), while a syringe pump (AcTIVA Prestige-equipment) fed the sol at a constant rate of 0.5 mL/h. The fibers were collected 10 cm below the needle tip over aluminum foil. The as-spun fibers were calcined in air for 1 h at different temperatures to obtain crystalline BaTiO₃ fibers (BT-fibers).

X-ray diffraction (XRD) was performed on fiber samples using a PANalytical, X'pert diffractometer with Cu K α radiation and step size of 0.02°/min, from 10° to 80° 2θ. Raman spectra were collected with a Renishaw inVia Raman Spectrometer by means of a 514 nm Ar-ion laser (50 mW nominal power). The microstructure and morphology of fibers was also characterized by field emission scanning electron microscopy (FE-SEM, Zeiss Supra 35).

A polymer–ceramic composite was prepared from bisphenol A type epoxy resin (D.E.R. 331) and D.E.H. 24 (12.5% w/w) curing agent, both from Dow Chemical, with Epolil 747 (10% w/w) as reactive diluent and tetrahydrofuran (THF, Dorwil Chemical) (10% w/w) as solvent. Heat-treated fiber mats were embedded into epoxy resin using silicone molds, and then composites were cured in an oven at 100 °C

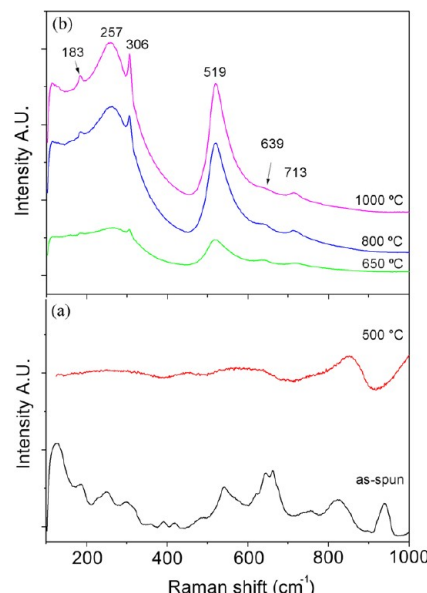


Figure 3. Raman spectra of barium titanate fibers heat-treated at different temperatures: (a) amorphous and (b) crystalline fibers.

for 2 h for solvent removing and resin polymerization. Cured samples were cut into 1 × 1 × 10 mm pieces.

For dielectric analysis, 1.0 × 10 mm opposite faces were coated with silver paint in order to obtain electrodes in two different configurations, perpendicular and parallel to the fiber layers as shown in Figure 1. A 1.0 × 1.0 × 10.0 mm epoxy piece was used as the reference sample. Thermogravimetric analyses were carried out in order to determine the ceramic fiber content of the composites using a Shimadzu TGA-50. Microphotographs were taken by scanning electron microscopy (SEM, Jeol JSM-6460LV) to reveal the composite microstructure, particularly in the polymer/fiber interphase. Dielectric measurements were carried out at room temperature in the 0.1–10⁷ Hz frequency range by means of HIOKI 3522-50 (10 mHz–100 kHz) and HIOKI 3535 (100 kHz–120 MHz) LCR HiTester units. Dielectric constant (ϵ) values were determined from capacitance (C_p), and loss tangent ($\tan \delta$) was also measured. In order to evaluate the influence of temperature, dielectric measurements were also performed on a Hewlett Packard 4284A LCR meter. Isothermal runs were carried out in the frequency domain 20 Hz–1 MHz from room temperature up to 100 °C, near the epoxy resin glass transition temperature (T_g).

RESULTS AND DISCUSSION

Figure 2 shows the XRD patterns of BaTiO₃ (BT) fibers heat-treated at different temperatures. Both as-synthesized and low temperature treated fibers showed amorphous structures. Samples treated at 650 °C and higher temperatures crystallized into

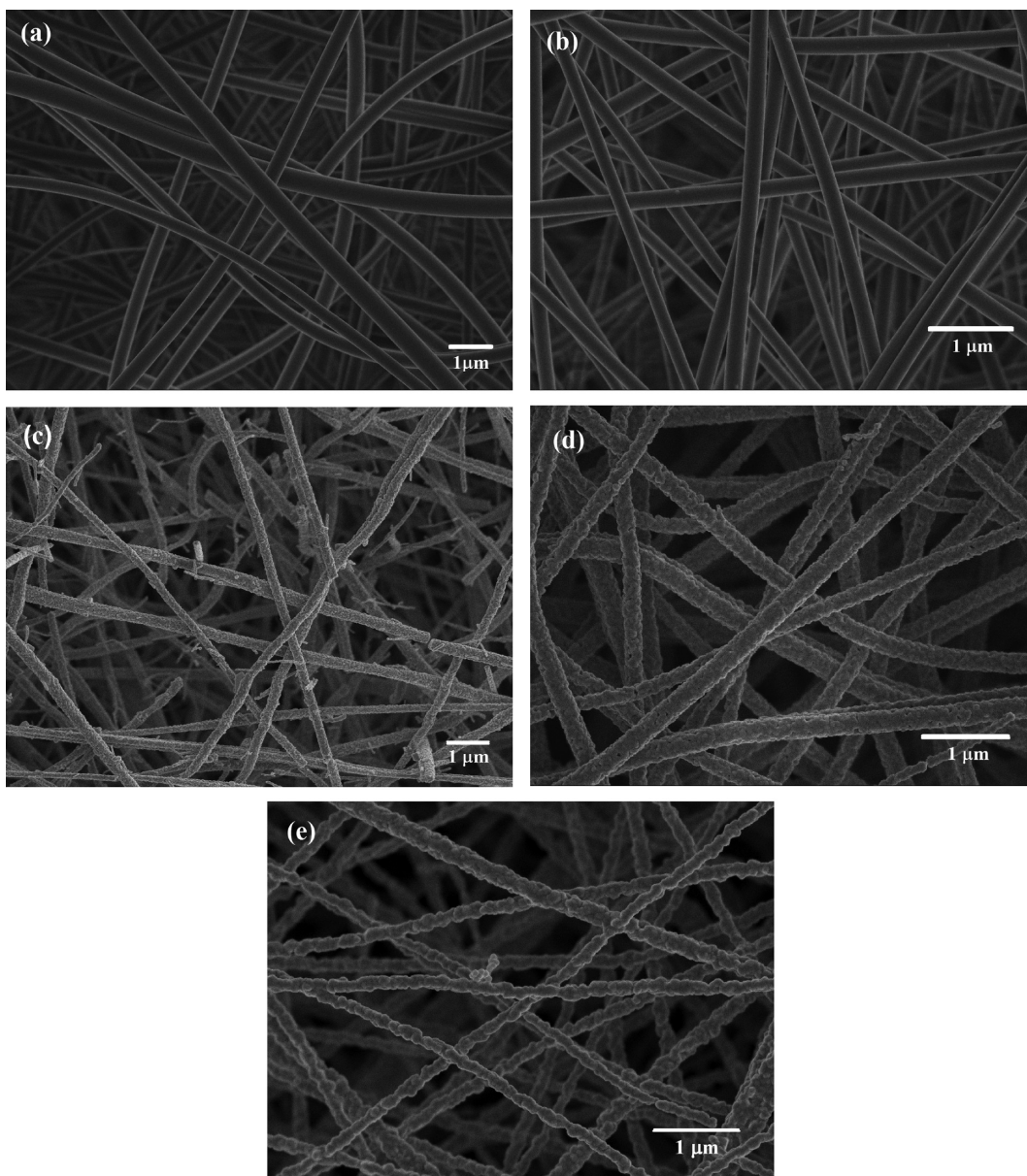


Figure 4. FE-SEM images of (a) PVP/BT as-spun fibers and fibers heat-treated at various temperatures: (b) 500 °C, (c) 650 °C, (d) 800 °C, and (e) 1000 °C.

perovskite BaTiO_3 in agreement with the JCPDS 74-1956 file. It can be observed that the characteristic splitting of the peaks corresponding to the (002) and (200) planes ($43\text{--}47^\circ 2\theta$) of the tetragonal phase did not occur.²⁶ On the other hand, a magnification of the $43\text{--}47.5^\circ 2\theta$ range (inset image in Figure 2) clearly shows differences in peak breadth of the sample heat-treated at 650 °C with respect to those treated at 800 and 1000 °C. The increase in peak breadth with increasing temperature is associated with a polar crystal structure and indicates an increasing degree of tetragonality. Moreover, the tetragonal structure was identified by Raman spectroscopy as shown in Figure 3. According to Figure 3a, the as-electrospun fibers exhibited different vibration modes corresponding to amorphous BT.³⁹ The electrospun BT fibers annealed at 500 °C resulted in amorphous BT fibers, which did not have active vibrational modes as shown also in Figure 3a. Samples annealed at temperatures above 650 °C showed bands associated with the vibration modes of the BT tetragonal phase, as can be seen

in Figure 3b.⁴⁰ However, it is worthwhile noting that the band at 639 cm^{-1} does not belong to the tetragonal phase of BaTiO_3 but is associated with high-temperature phases of the $\text{BaO}\text{--}\text{TiO}_2$ system.⁴¹ The vibration modes associated with these signals have been discussed in a previous work.⁴²

Figure 4 shows the FE-SEM images of as-electrospun and heat-treated fibers. The as-electrospun fibers are uniform in diameter as well as samples heat-treated at 500 °C. The average diameter of as-electrospun fibers is 360 nm (Figure 4a), whereas that of fibers annealed at 500 °C is 290 nm (Figure 4b). These fibers have quite smooth surfaces due to the amorphous nature of BaTiO_3 . After heat-treatments above 650 °C, the fibers consisted of sintered particles which maintained their fibrous structures as shown in Figure 4c–e. At higher temperatures, the crystallinity of the fibers was improved and the grain size grew along the fibers. Figure 4c,d shows fibers heat-treated at 650 and 800 °C with average diameters of 246 and 210 nm, respectively. Interestingly, the nanofibers heat-treated

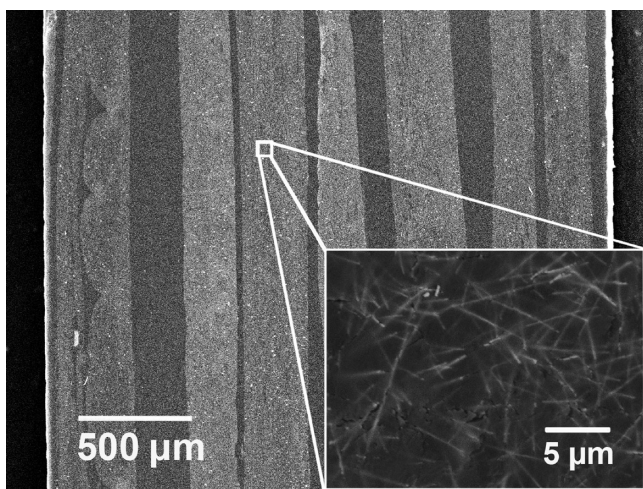


Figure 5. Cross-sectional SEM image of an epoxy/BT-fiber composite showing fiber layers (vertical bright regions) embedded in epoxy resin (dark regions). The inset corresponds to a magnification of the framed region.

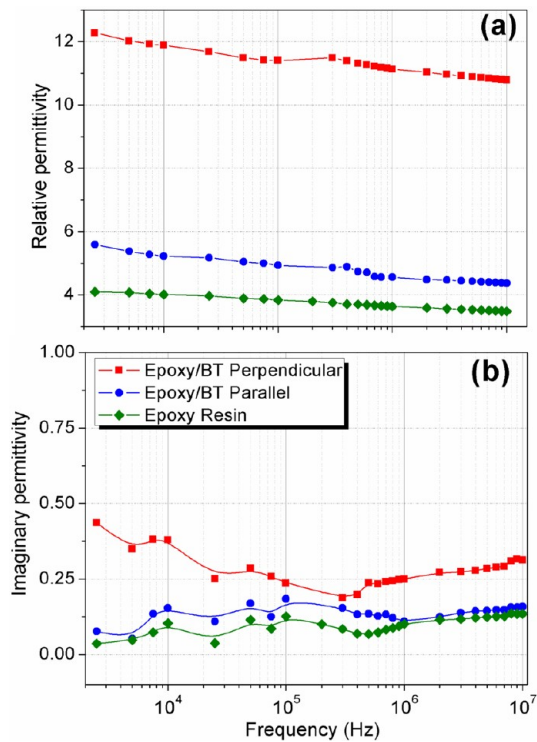


Figure 6. Relative (a) and imaginary (b) permittivity of epoxy resin and epoxy resin/BT-fiber composites.

at 1000 °C (Figure 4e) clearly consist of linked particles of almost the same size as the fiber diameter (167 nm).

Figure 5 shows a cross-section image of epoxy/BT-fiber composite made up with fibers heat treated at 800 °C. The micrograph shows dark and bright regions that belong to the epoxy resin matrix and BT fiber layers, respectively. Ceramic fibers, which are entirely embedded in epoxy resin, can be observed in the inset of Figure 5. It is clear that the epoxy resin fully covers the fibers mats and that the presence of voids or porosity in epoxy/BT-fibers interphase is negligible. By means of thermogravimetric analysis, it was determined that the samples are composed of 2 vol % BaTiO₃.

Table 1. Permittivity Values Measured at Room Temperature and 100 kHz of Epoxy Resin and Epoxy/BT-Fiber Composites with Electrodes Parallel and Perpendicular to the Fiber Layers

sample	relative permittivity (ϵ')	imaginary permittivity (ϵ'')
epoxy resin	3.86 ± 0.30	0.12 ± 0.05
epoxy/BT fibers—parallel	4.97 ± 0.6	0.18 ± 0.06
epoxy/BT fibers—perpendicular	11.41 ± 0.75	0.24 ± 0.13

The relative (real part) and imaginary permittivity of epoxy resin and epoxy/BT-fibers composites with perpendicular and parallel electrode configurations were measured at room temperature. These results are shown in Figure 6 and summarized in Table 1. The perpendicular epoxy/BT-fibers composite showed higher relative permittivity values than the parallel epoxy/BT-fibers composite and epoxy resin (Figure 6a). The relative permittivity of the perpendicular composite is almost three times higher than that of the pure epoxy sample. This is a significant improvement, considering the low content of ceramic fibers.

The higher permittivity of samples with electrodes perpendicular to the BT-fiber layers is attributed to the orientation of layers in the polymer matrix. The electric field flows through the ceramic fibers following the easier path provided by them and subsequently a higher dielectric permittivity is attained.³⁶ On the other hand, the epoxy/BT-fibers parallel composite showed low permittivity values, which is however higher than those measured for the epoxy resin sample due to the presence of the ceramic phase. As shown in Figure 6b, the perpendicular epoxy/BT-fibers composite showed higher imaginary permittivity than the other samples. However, losses are quite low in the whole frequency range for both composites and epoxy resin.

Figure 7 shows the relative and imaginary permittivity as a function of temperature measured at 100 kHz. Figure 7a shows that relative permittivity for composite increases with temperature up to 80 °C, approximately. According to Hammami et al., at temperatures close to the epoxy glass transition ($T_g \sim 94$ °C) the dipoles gain enough mobility to contribute to the permittivity.³⁶ The imaginary permittivity for epoxy/BT-fiber composites reaches a maximum value at 80 °C as a result of ceramic content and high mobility of polymeric chains near the T_g (α -relaxation),³⁷ whereas the permittivity of the epoxy resin sample only depends on the polymer segmental mobility.

Figure 8 shows the real (M') and the imaginary (M'') parts of the electric modulus (M^*) for epoxy resin and epoxy/BT-fiber composites measured at 80 and 100 °C in the 20 Hz⁻¹ MHz frequency range. This figure shows that M' values increase quickly with frequency until they reach an almost constant value. In the same frequency range, M'' curves show peaks that indicate a relaxation process which is also evident in the curves of the imaginary part of permittivity (Figure 7b). This peak corresponds to the α relaxation and takes place at high temperature, near the epoxy resin T_g , as the mobility of polymer molecules is enhanced.^{36,38}

In general, the three systems present similar behaviors. Nevertheless, perpendicular epoxy/BT-fiber composites showed smaller M' and M'' values than the other samples. The orientation of the fiber layers with respect to the electrodes and temperature shift the frequency of the α relaxation. Considering that interfacial or Maxwell-Wagner-Sillars (MWS) relaxations are commonly observed in these kinds of composites,⁴³ com-

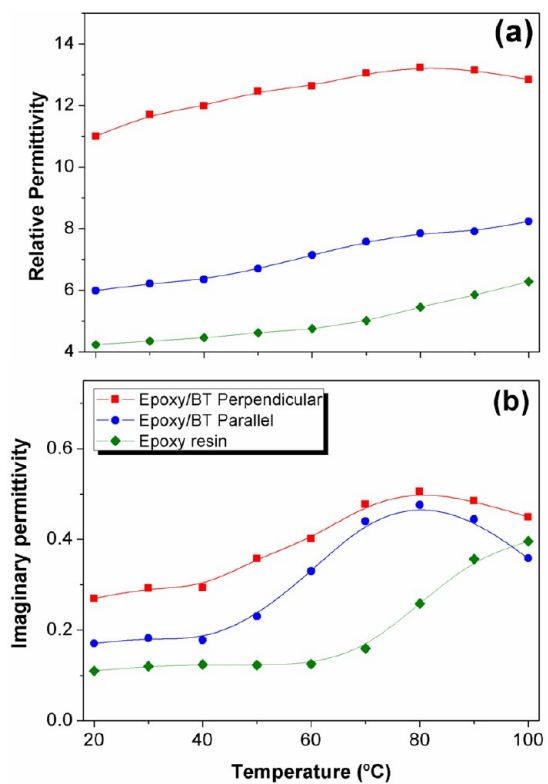


Figure 7. Relative (a) and imaginary (b) permittivity vs temperature curves measured at 100 kHz.

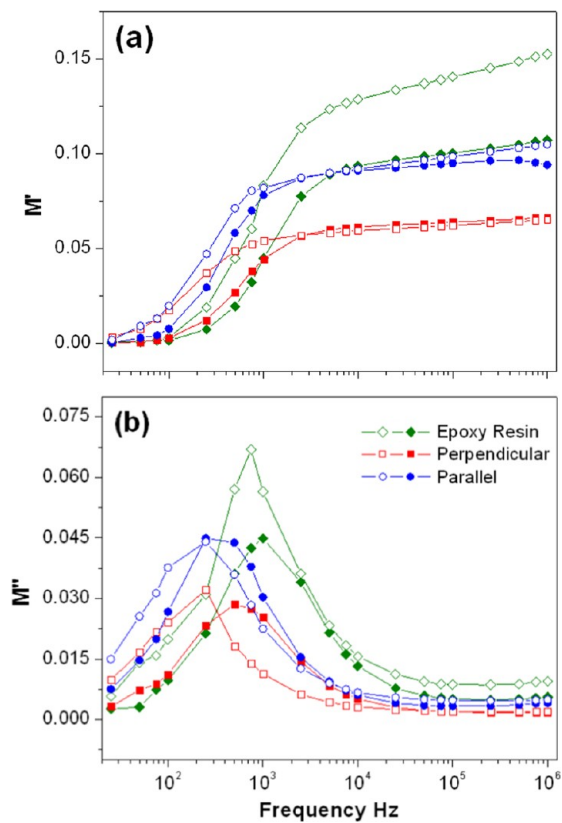


Figure 8. (a) Real (M') and (b) imaginary (M'') components of the dielectric modulus vs frequency curves for epoxy resin and epoxy/BT-fiber composites. Empty and filled symbols correspond to 80 and 100 °C, respectively.

Table 2. Electrical Parameters of Epoxy/BT Composites with Different Ceramic Content As Reported in the Literature

vol % BT	relative permittivity	loss tangent	frequency	reference
10	13	0.021	100 kHz	44
20	14	0.028	100 kHz	44
25	11.8	N/A	100 kHz	45
20	11	N/A	100 kHz	32
20	11	N/A	100 kHz	46
30	14	0.010	2.5 kHz	38
45	13.1	0.025	1 GHz	31
30	12	0.020	1 MHz	35
40	13.9	0.020	1 MHz	47
2	11.4	0.012	100 kHz	this work

plex modulus plots in Figure 8 show a slight interfacial polarization due to the low ceramic content in the composites under study.

In this work a straightforward method for the synthesis of BaTiO₃ nanostructured fibers and their use in epoxy-based composite materials for electronic applications was presented. In order to put the results in a comparative frame, Table 2 shows relative permittivity and loss tangent values reported by different authors for epoxy resin/BaTiO₃ composites. In the cited works, the permittivity was seen to increase with BT particle content and size, attaining maximum permittivity values for composites with BT volume fractions of 50–60% with particle size in the micrometer scale. In contrast, in this work almost the same permittivity was measured for composites with a 2% ceramic volume fraction, using nanostructured electrospun fibers of submicrometric grain size (0.2 μ m) and fiber mats arranged perpendicularly to the electrodes. It is worthwhile to note that, with respect to the cited works, the amount of ceramic filler was reduced 5–10 times and a composite material with permittivity three times higher than that of pure epoxy resin was achieved.

CONCLUSIONS

BaTiO₃ nanostructured fibers have been synthesized by sol–gel and electrospinning. XRD revealed that completely crystalline BaTiO₃ fibers are obtained with thermal treatments above 650 °C, and Raman spectroscopy confirmed the presence of the BaTiO₃ tetragonal phase. FE-SEM images showed that the fiber structure was maintained when the annealing temperature was increased from 650° to 1000 °C. At high temperatures the fiber diameter decreased and fibers exhibited rougher surfaces due to grain formation. The low porosity observed in epoxy/BT-fiber composites confirmed the compatibility between epoxy resin and BT-fibers. The relative and imaginary permittivity values were influenced significantly by the electrode configuration with respect to the fiber layers. Samples with perpendicular electrodes showed permittivities 3 times higher than pure resin samples and almost twice that of the sample with electrodes parallel to the BT layers in the whole frequency range. Epoxy resin and parallel BT-fiber composites showed similar dielectric properties. Using the electric modulus formalism, the α -relaxation process of epoxy/BT-fiber composites and epoxy resin could be verified. The Maxwell-Wagner-Sillars (MWS) relaxation due to the presence of ceramic/polymer interface was not clearly observed because of the low ceramic content in epoxy/BT-fibers composites.

AUTHOR INFORMATION

Notes

The authors declare no competing financial interest.

ACKNOWLEDGMENTS

This work was carried out with the financial aid of CONICET, ANCyPT, and UNMdP. Also, L'Oréal - UNESCO "For Women in Science" Program is acknowledged.

Thanks are due to Prof. G. A. Abraham for access to electrospinning facilities, suggestions, and fruitful discussions.

REFERENCES

- (1) Ramaseshan, R.; Sundarajan, S.; Jose, R.; Ramakrishna, S. *J. Appl. Phys.* **2007**, *111*, 11101.
- (2) Ding, B.; Wang, M.; Yu, J.; Sun, G. *Sensors* **2009**, *9*, 1609–1624.
- (3) Lu, X.; Wang, C.; Wei, Y. *Small* **2009**, *5*, 2349–2370.
- (4) Lu, X.; Zhang, W.; Wang, C.; Wen, T.-C.; Wei, Y. *Prog. Polym. Sci.* **2011**, *36*, 671–712.
- (5) Kuchibhatla, S. V. N. T.; Karakoti, A. S.; Bera, D.; Seal, S. *Prog. Mater. Sci.* **2007**, *52*, 699–913.
- (6) Wu, X.; Wang, L.; Yu, H.; Huang, Y. *J. Appl. Polym. Sci.* **2005**, *97*, 1292–1297.
- (7) Frey, M. W. *Polym. Rev.* **2008**, *48*, 378–391.
- (8) Sui, X.; Yuan, J.; Yuan, W.; Zhou, M. *Chem. Lett.* **2008**, *37*, 114–115.
- (9) Tuttle, R. W.; Chowdury, A.; Bender, E. T.; Ramsier, R. D.; Rapp, J. L.; Espe, M. P. *Appl. Surf. Sci.* **2008**, *254*, 4925–4929.
- (10) Wang, S.; Li, Y.; Wang, Y.; Yang, Q.; Wei, Y. *Mater. Lett.* **2007**, *61*, 4674–4678.
- (11) Batool, S. S.; Imran, Z.; Rafiq, M. A.; Hasan, M. M.; Willander, M. *Ceram. Int.* **2012**, *39*, 1775–1783.
- (12) Li, D.; Xia, Y. *Nano Lett.* **2003**, *3*, 555–560.
- (13) Hayat, K.; Rafiq, M. A.; Hasan, M. M. *Ceram. Int.* **2012**, *38*, 1441–1445.
- (14) Kim, I.-D.; Rothschild, A.; Lee, B. H.; Kim, D. Y.; Jo, S. M.; Tuller, H. L. *Nano Lett.* **2006**, *6*, 2009–2013.
- (15) Kim, I.-D.; Jeon, E.-K.; Choi, S.-H.; Choi, D.-K.; Tuller, H. L. *Electroceram.* **2010**, *25*, 159–167.
- (16) Landau, O.; Rothschild, A.; Zussman, E. *Chem. Mater.* **2009**, *21*, 9–11.
- (17) Liu, Z.; Sun, D. D.; Guo, P.; Leckie, J. O. *Nano Lett.* **2007**, *7*, 1081–1085.
- (18) Berutti, F. A.; Alves, A. K.; Clemens, F. J.; Graule, T.; Bergmann, C. P. *Adv. Appl. Ceram.* **2010**, *109*, 62–64.
- (19) Zhan, S.; Yu, H.; Li, Y.; Jiang, B.; Zhang, X.; Yan, C.; Ma, S. *J. Dispersion Sci. Technol.* **2008**, *29*, 1345–1348.
- (20) Yuh, J.; Perez, L.; Sigmund, W. M.; Nino, J. C. *Physica E* **2007**, *37*, 254–259.
- (21) Yuh, J.; Perez, L.; Sigmund, W. M.; Nino, J. C. *J. Sol-Gel Sci. Technol.* **2007**, *42*, 323–329.
- (22) Yuh, J.; Nino, J. C.; Sigmund, W. M. *Mater. Lett.* **2005**, *59*, 3645–3647.
- (23) Li, H.; Sun, Y.; Zhang, W.; Pan, W. *J. Alloys Compd.* **2010**, *508*, 536–539.
- (24) Maensiri, S.; Nuansing, W.; Klinkaewnarong, J.; Laokul, P.; Khemprasit, J. *J. Colloid Interface Sci.* **2006**, *297*, 578–583.
- (25) Wang, L.; He, Y.; Hu, J.; Qi, Q.; Zhang, T. *Sens. Actuators, B* **2011**, *153*, 460–464.
- (26) Li, H.; Wu, H.; Lin, D.; Pan, W. *J. Am. Ceram. Soc.* **2009**, *92*, 2162–2164.
- (27) McCann, J. T.; Chen, J. I. L.; Li, D.; Ye, Z.-G.; Xia, Y. *Chem. Phys. Lett.* **2006**, *424*, 162–166.
- (28) Mimura, K.-I.; Moriya, M.; Sakamoto, W.; Yogo, T. *Compos. Sci. Technol.* **2010**, *70*, 492–497.
- (29) Baji, A.; Mai, Y.-W.; Li, Q.; Liu, Y. *Compos. Sci. Technol.* **2011**, *71*, 1435–1440.
- (30) Kumar, B.; Fellner, J. P. *J. Power Sources* **2003**, *123*, 132–136.
- (31) Cheng, K.-C.; Lin, C.-M.; Wang, S.-F.; Lin, S. T.; Yang, C.-F. *Mater. Lett.* **2007**, *61*, 757–760.
- (32) Cho, S.-D.; Lee, J.-Y.; Hyun, J.-G.; Paik, K.-W. *Mater. Sci. Eng. B* **2004**, *110*, 233–239.
- (33) Kobayashi, Y.; Kosuge, A.; Konno, M. *Appl. Surf. Sci.* **2008**, *255*, 2723–2729.
- (34) Xie, S.-H.; Zhu, B.-K.; Wei, X.-Z.; Xu, Z.-K.; Xu, Y.-Y. *Composites, Part A* **2005**, *36*, 1152–1157.
- (35) Dang, Z.-M.; Yu, Y.-F.; Xu, H.-P.; Bai, J. *Compos. Sci. Technol.* **2008**, *68*, 171–177.
- (36) Hammami, H.; Arous, M.; Lagache, M.; Kallel, A. *J. Alloys Compd.* **2007**, *430*, 1–8.
- (37) Ramajo, L.; Castro, M. S.; Reboreda, M. M. *Composites, Part A* **2007**, *38*, 1852–1859.
- (38) Ramajo, L.; Castro, M. S.; Reboreda, M. M. *Composites, Part A* **2005**, *36*, 1267–1274.
- (39) Tanaka, N.; Kensaku Ito, K.; Kitano, H. *Macromol. Chem. Phys.* **1994**, *195*, 3369.
- (40) Clark, I. J.; Takeuchi, T.; Ohtori, N.; Sinclair, D. C. *J. Mater. Chem.* **1999**, *9*, 83–91.
- (41) He, Q.-Y.; Tang, X.-G.; Zhang, J. X.; Wu, M.-M. *Nanostruct. Mater.* **1999**, *11*, 287–293.
- (42) Ávila, H. A.; Ramajo, L. A.; Reboreda, M. M.; Castro, M. S.; Parra, R. *Ceram. Int.* **2011**, *37*, 2383–2390.
- (43) Hammami, H.; Arous, M.; Lagache, M.; Kallel, A. *Composites, Part A* **2006**, *37*, 1–8.
- (44) Kuo, D.-H.; Chang, C.-C.; Su, T.-Y. *J. Eur. Ceram. Soc.* **2001**, *21*, 1171–1177.
- (45) Orlowska, S.; Beroual, A.; Fleszynski, J. *J. Phys. D: Appl. Phys.* **2002**, *35*, 2656–2660.
- (46) Cho, S.-D.; Lee, S.-Y.; Hyun, J.-G.; Paik, K.-W. *J. Mater. Sci. Mater. Electron.* **2005**, *16*, 77–84.
- (47) Das, R. N.; Lauffer, J. M.; Markovich, V. R. *J. Mater. Chem.* **2008**, *18*, 537–544.